

Time-resolved and time-integrated photoluminescence analysis of state filling and quantum confinement of silicon quantum dots

Lap Van Dao,^{a)} Xiaoming Wen, My Tra Thi Do, and Peter Hannaford
Centre for Atom Optics and Ultrafast Spectroscopy, School of Biophysical Sciences and Electrical Engineering, Swinburne University of Technology, Melbourne 3122, Australia

Eun-Chel Cho, Young H. Cho, and Yidan Huang
Centre of Excellence for Advanced Silicon Photovoltaics and Photonics, The University of New South Wales, Sydney, New South Wales 2052, Australia

(Received 11 August 2004; accepted 29 September 2004; published online 13 December 2004)

In this paper we report studies of the optical properties of silicon quantum dot structures. From time-resolved and time-integrated photoluminescence measurements we investigate the state-filling effect and carrier lifetime, and discuss the parabolic confinement of quantum dot structures and the large energy splitting between quantum dot levels. The photoluminescence intensities for different quantum dot levels decay with a stretched exponential function and the decay times are in the range 2–100 μs depending on the observation wavelength and the dot size. © 2005 American Institute of Physics. [DOI: 10.1063/1.1823027]

I. INTRODUCTION

Recently, the optical properties of low dimensional quantum structures such as quantum dots (QDs) have attracted wide interest and discussion because of the physical interest and their technological applications. The δ -function density of states in QDs leads to a rapid reduction of inter-level scattering rates because of the so-called phonon bottleneck,^{1,2} but it has been shown that the short relaxation times can be explained by considering multiphonon processes² and Auger processes.³ The state-filling effect⁴ has been observed in several experiments where the excited-state luminescence begins to be observed at a higher excitation density because the lower energy states with low density of states are occupied. The carrier relaxation and dynamics are interesting topics for studying the optical properties and applications of QDs.

The efficient light emission from silicon (Si) nanostructures⁵ involving quantum confinement effects has led to the current interest in Si for optoelectronic devices. Because Si is the most technologically important material this century a light-emitting Si device could result in a new generation of Si technology from microelectronics to optoelectronics. Light emission from silicon, which is an indirect band-gap semiconductor, is possible in Si nanocrystals because of quantum confinement. The quantum confinement in nanocrystals of Si causes an enlargement of the band gap and efficient emission in the visible range at room temperature.

In this paper we present results of the study of the optical properties of Si QD structures. Using time-resolved and time-integrated measurements we study the state-filling effect which leads to discussion about the parabolic confinement of quantum dot structures and the splitting of the energy levels. The photoluminescence (PL) intensity decays

with a stretched exponential function and the decay times are in the range 2–100 μs , which depends on the observed energy levels and dot sizes.

II. SAMPLE STRUCTURES

An excess of silicon in substoichiometric oxide, also known as silicon rich oxide (SRO), i.e., $\text{SiO}_x (x < 2)$, generates Si precipitations attributed to the diffusion of Si atoms leaving the stoichiometric oxide (SiO_2) during high temperature thermal annealing.⁶ A deposited SRO film is thermodynamically unstable below 1173 °C and phase separation and diffusion of the Si atoms in the amorphous SiO_2 matrix creates nanoscale Si quantum dots.⁶ The size of the Si dots depends on the thermal budget, film thickness, and stoichiometry of the SRO. In our experiment the Si QD superlattices were fabricated by alternate deposition of silicon oxide and SRO with differing thicknesses. The conventional furnace annealing under a nitrogen atmosphere (1100 °C, 1 h) was performed to precipitate Si and nanocrystalline Si growth by the diffusion of silicon in the oxide.⁷ Only lateral Si diffusion and Si grain growth occurs in thin SRO films enclosed by amorphous silicon oxide so that the maximum size of the Si quantum dots is determined by the SRO thickness. Figure 1(a) shows a transmission electron microscopy (TEM) image of eight layers of Si quantum dots in an oxide matrix, where the dots in the white region (glue) originate from particles during the TEM sample preparation. Two shapes of quantum dots (of about 4 nm diameter), spherical dots and near-spherical dots, with the same vertical thickness were observed in high-resolution TEM (HRTEM) images favored by the surface energy minimization, which is thermodynamically stable. A typical HRTEM image is shown in Fig. 1(b). The size of the Si quantum dots was controlled by the deposition time and other optimal sputtering parameters (gas mixing ratio, deposition pressure, and rf power). The spacing or distance between the dots is determined by the amount of silicon in the SRO layer. Two samples have been

^{a)}Author to whom correspondence should be addressed; FAX: +61392145840; electronic mail: dvlap@swin.edu.au

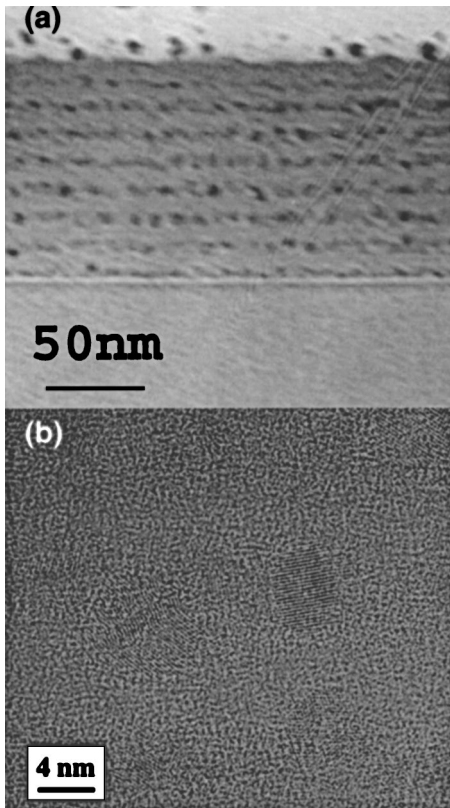


FIG. 1. TEM images of a Si quantum dot superlattice with eight bilayers of Si dots and SiO₂ (a) and its lattice image (b).

used for this study with an average dot size distribution of 3.4 nm (sample s92) and 4.3 nm (sample s106, which is on sapphire substrate) and the dot density is about 10^{12} – 10^{13} dots/cm².

III. EXPERIMENTS

Time-resolved and time-integrated PL signals are used to study the optical properties of the samples. The PL signal is dispersed by a 0.27 m grating spectrometer and detected with a photomultiplier (PMT). The sample was mounted in a closed-cycle helium cryostat with a variable temperature ranging from 15–300 K. In the time-integrated PL measurements the spectra were recorded using a lock-in amplifier. For the time-resolved measurements the response function of the PMT is reduced to reach a time resolution of about 5 ns, which is much shorter than the decay time of the signals (in the microsecond range) and the signal is recorded by a 500 MHz (5 Gs/s) digital oscilloscope or a boxcar system. Femtosecond laser pulses with a duration of 100 fs and a repetition rate of 1 kHz are used for the excitation. The femtosecond pulses are generated by the conversion of a 1 mJ amplified pulse (80 fs, 800 nm) in a tunable optical parametric amplifier that covers a wide range of wavelengths (200–2000 nm) with high pulse energy (1–100 μ J/pulse).

In this work the PL spectra of the QDs taken at an excitation wavelength of 400 nm, which is well above the band gap of the Si QDs, and the excited carriers are generated in the SRO layer or very high excited states of the QDs. The energy of the excitation laser pulse varies from 0.05 to 2 μ J

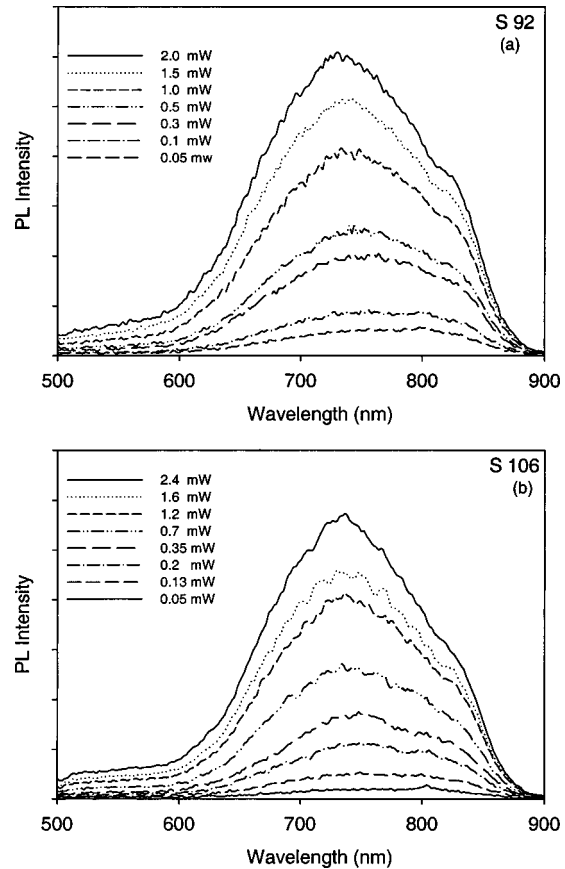


FIG. 2. Time-integrated spectrum of Si quantum dot sample measured at different excitation intensity (a) for sample s92 with 3.4 nm dot size and (b) for sample s106 with 4.3 nm dot size.

with a photon density of about 10^{13} – 10^{15} photons/cm². Under these conditions at high excitation energy we expect that more than 10 electrons/dot can be generated.

IV. RESULTS AND DISCUSSION

Figures 2(a) and 2(b) show PL spectra of two samples at room temperature taken at different excitation intensities. A very broadband (\sim 350 meV) PL signal around 750 nm with no clear structure⁸ is observed. The emission involves electron-hole recombination between distinct QD states in the conduction band (CB) and the valence band (VB). When the excitation intensity is increased the PL intensity of the low energy part of the spectrum (800 nm, 850 nm) increases more slowly than that of the high energy part and a small shift of the maximum of the PL spectrum is observed (780 nm for 0.05 μ J excitation and 750 nm for 2 μ J). A slight difference in the peak position and bandwidth can be seen in the spectrum of the two samples. Because the spectrum is very broad and the peaks due to recombination of carriers in different energy levels cannot be clearly resolved, we evaluate the PL intensity for different levels by recording the spectrally integrated signal with a spectral window of 2 nm in 50 nm steps across the spectrum (600–850 nm). The results are shown in Fig. 3(a) for sample s92 and Fig. 3(b) for sample s106, e.g., for three different wavelengths 650 nm, 750 nm, and 850 nm. The dependence of the PL intensity on excitation intensity and saturation of PL inten-

sity is different for different detection wavelengths. According to the state-filling effect, lower energy levels with a low density of states will become saturated at low intensity as the higher energy levels will be still populated as the excitation intensity increases.

For a quantitative analysis of the PL measurements we use a simple coupled rate equation model.^{9,10} The PL intensity for a given transition i is proportional to the density of electron and hole pairs in the relevant energy level. The holes are probably present in the dots prior to the optical excitation pulse and we can describe the PL intensity as proportional to the density N_i of electrons in level i of the CB. The carrier relaxation to level i from a higher level ($j > i$) is proportional to the nonoccupancy of this level. The rate equation for a particular energy level i can be written as

$$\frac{dN_i(t)}{dt} = -\frac{N_i(t)}{\tau_{lf}^i} + \sum_{j>i} \frac{N_j(t)}{\tau_{rel}^{ji}} \frac{D_i - N_i(t)}{D_i} - \sum_{j<i} \frac{N_i(t)}{\tau_{rel}^{ij}} \frac{D_j - N_j(t)}{D_j} + G_i(t), \quad (1)$$

where $G_i(t)$ is the population generated by the laser directly or captured from outside the dots, τ_{lf}^i is the effective lifetime of the i th level, and τ_{rel}^{ij} is the relaxation time between dots in levels i and j . The factor $(D_i - N_i)/D_i$ (where D_i is the density of states of level i) is a state-filling factor which allows for the fact that electrons can only relax to a lower-lying unoccupied dot level (Pauli blocking). Due to the increase of the relaxation pathway from a given level with increasing i , the decay of $N_i(t)$ becomes faster for high i values. For a structure with level degeneracy g_i and dot density D_d we can write $D_i = g_i D_d$.

If the energy relaxation rate constant $1/\tau_{rel}^{ij}$ is efficient enough, according to the rate equation (1) there will be no luminescence from the excited states as long as the low-lying level is not saturated. The observation of luminescence from higher-excited states before the lower-energy states are saturated can be treated as a result of the influence of phonon bottleneck effects. Grundmann and Bimberg¹¹ on the basis of theoretical calculations argue that the excited states will appear before saturation of the lower levels even for very short relaxation time. It has been shown that the state-filling effect would hinder the interlevel scattering rate.¹⁰ At room temperature the energy separation between the energy states is small compared to kT and thermalization of the carriers becomes significant and then the interdot coupling would make the capture and recombination processes more complex. The small shift of the PL spectrum when the excitation intensity is increased by nearly two orders of magnitude suggests a low interlevel relaxation rate in our sample.

The coupled rate equation (1) for multilevel dots cannot be solved analytically. In the simple case, which is useful for interpretation of the excitation intensity dependence, the interlevel relaxation rate is small. Then for excitation into the barriers layer without considering saturation of the absorption processes the rate equation can be written in the simple form

$$\frac{dN_i(t)}{dt} = -\frac{N_i(t)}{\tau_{lf}^i} + \frac{\sigma I N_0 [D_i - N_i(t)]}{\tau_{cap}^i D_i}, \quad (2)$$

where τ_{cap}^i is the capture time of the carriers of the dot levels i , σ is the absorption cross section, N_0 is the total density of states in the wetting layer, and I is the laser intensity. Under stationary or quasistationary conditions ($dN_i/dt=0$), the population of level i can be deduced by

$$N_i \sim D_i / (1 + \alpha_i D_i / I) \text{ with } \alpha_i = \tau_{cap}^i / (\sigma N_0 \tau_{lf}^i), \quad (3)$$

where $\alpha_i D_i$ is the saturation factor which depends on the optical properties of level i . A similar solution can be obtained for the time-integrated population density of level i . The time-integrated luminescence intensity I_{PL}^i at a given wavelength for recombination of electrons or holes from level i can be written

$$I_{PL}^i \sim \eta_i N_i \sim \eta_i D_i / (1 + \alpha_i D_i / I), \quad (4)$$

where η_i is the quantum efficiency.

The QD energy level can be described by a harmonic oscillator model for parabolic quantum confinement.¹¹ The potential function can be written as $V_j = m^* \omega_j^2 r^2 / 2$, where j represents an electron or a hole, ω_j is the frequency, m^* is the effective mass, and r is the radial coordinate of the dot. The eigenenergies for a single electron or hole are $E_{lm}^j = \hbar \omega_j (2\ell - |m| + 1)$ where ℓ is the radial quantum number, m is the angular momentum quantum number, and \hbar is Planck's constant. We can set $i = 2\ell - |m|$ in which case the eigenenergy is of the form $E_i^j = \hbar \omega_j (i + 1)$. If we take the spin degeneracy into account the degeneracy of each state is $g_i = 2(i + 1)$, with $i = 0, 1, 2, \dots$.

Equation (4) provides a good fit for the intensity dependence of the PL at different wavelengths, as shown by the solid line in Fig. 3. The saturation factor ($\alpha_i D_i$) increases with increase of detection photon energy. Considering the ratio $\tau_{ca}^i / \tau_{lf}^i$ can be independent of or weakly dependent on the dot levels we deduce the degeneracy of the energy level in the quantum dot from the saturation parameter ($\alpha_i D_i / \alpha_0 D_0 \sim g_i / 2$) where $\alpha_0 D_0$ is the saturation parameter of the ground level ($i=0$). The results calculated from fitting of saturation parameter are shown in the insets of Figs. 3(a) and 3(b) for the two samples and are represented by the symbol (●), when the ground level luminescence is observed at 850 nm.

To gain insight into the relaxation and recombination scenario we have performed time-resolved PL experiments. We adjusted the excitation intensity for the PL spectrum to be comparable to the high-intensity spectrum, as shown in Fig. 2. This allows investigation of the carrier relaxation dynamics between distinct QD levels starting with several fully occupied QD levels (we suggest that we can generate more than 10 electrons/dot). We measure the PL intensity at different wavelengths and take the ratio of the intensity for each short wavelength (I_λ) to the maximum intensity for 850 nm (I_0), which would be seen as luminescence from the ground dot level. Figure 4 shows the PL intensity for different wavelengths with a step of 50 nm in the first 5 μ s after excitation. The rise times of all recorded signals are limited by the temporal resolution of the detection system. This

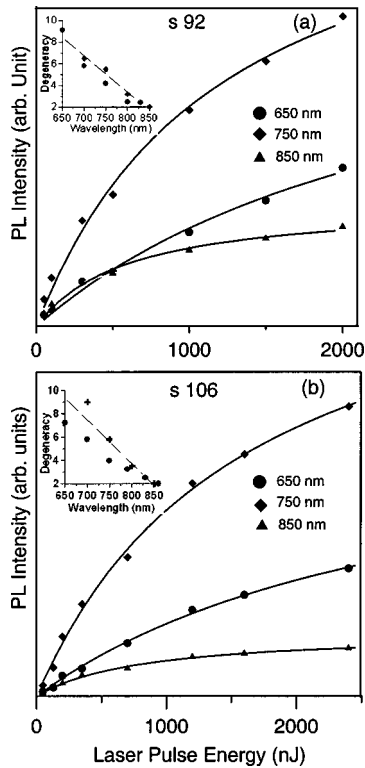


FIG. 3. Intensity dependence of PL intensity taken from Fig. 2 with spectral window 2 nm for different detection wavelength [(▲) 850 nm, (◆) 750 nm, and (●) 650 nm]. The symbols are the experimental data. The lines represent the fit using Eq. (4). The insets show the degeneracy calculated from fitting the saturation factor (●) and maximum PL intensity (+).

shows that the capture time is shorter than 5 ns. The maximum of the PL intensity reflects the “filling” of the dot levels by photon-excited carriers and depends on the density of states of given dot levels. In the short time after excitation, when the PL intensity is expected to reach the maximum, the influence of recombination and relaxation is very small and the dependence of the maximum PL intensity can be determined by Eq. (2) with $\tau_j \gg \tau_{cap}$. When the capture rate is independent of the dot energy level, following Eq. (2) we find the ratio $I_\lambda^{\max}/I_0^{\max} \sim g_i$, where I_0^{\max} is the maximum of the PL intensity of the ground dot level (850 nm) and I_λ^{\max} is the maximum of the PL intensity at a given wavelength. The calculated results of g_i are displayed in the inset of Fig. 3 by the symbol (+).

The degeneracy is close to $g_n=2(n+1)$ [the dashed line in the inset of Figs. 3(a) and 3(b) is an aid to the eye] which shows that a parabolic potential is a good approximation for these QD structures. From the intensity dependence of the PL spectrum we can explain that the PL around 850–800 nm is due to transitions involving the dot ground level ($n=0$) which shifts to longer wavelength for sample s106 with large dot size [see the insets of Fig. 3(a) and 3(b)]. The PL at shorter wavelength involves recombination of electrons and holes from high excited levels ($n \geq 1$). The energy splitting between the levels (taken with $g_i=2,4,6,\dots$) is about 90 meV (~ 45 nm) for s92 with 3.4 nm dot size and 75 meV (~ 40 nm) for s106 (4.3 nm dot size), which are much larger than the splitting of the dot levels in $A^{III}B^V$ materials [<50 meV (Ref. 12)].

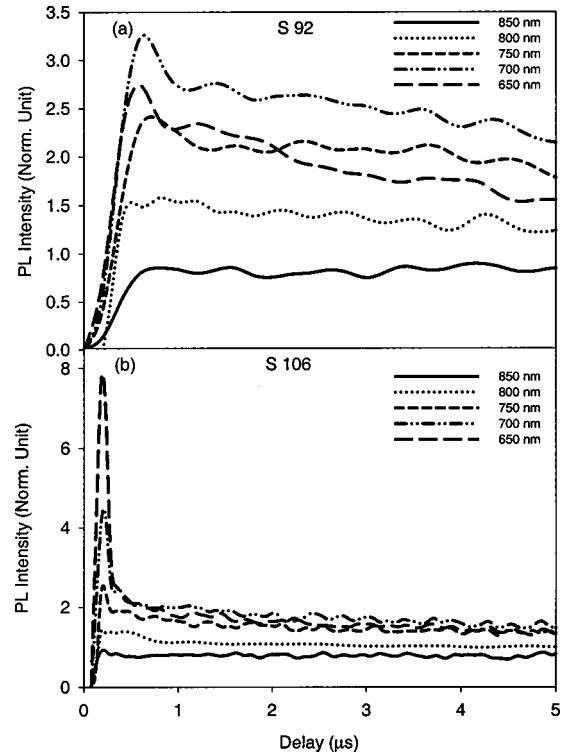


FIG. 4. PL intensity vs time delay in the first 5 μ s after excitation for different detection wavelengths, and (a) for sample s92 and (b) for sample s106. The intensity for different wavelengths is normalized to maximum intensity of the PL intensity at 850 nm.

In the transmission measurement for the sample with a sapphire substrate (s106) we do not find detectable absorption for wavelengths in the spectral region of the QD transition. This is probably due to the fact that the QD states in the VB are at least partly occupied by holes. If this assumption is correct the PL dynamics should be determined mainly by relaxation of electrons in the CB.

Figure 5 shows a nonexponential PL decay for the s92 sample taken at different detection wavelengths. In order to analyze the temporal evolution of the PL we have fitted the decay signals to a stretched-exponential function¹⁵ which is frequently used to describe dispersive processes in disordered systems having a distribution of relaxation times, and is given by

$$I(t) = I_0 \exp[-(t/\tau)^\beta], \quad (5)$$

where τ is the PL lifetime and $0 \leq \beta \leq 1$ is the dispersion exponent. The solid lines in Fig. 5 represent the best fit of the experimental data to Eq. (5). We can see that a very good fit is obtained for all wavelengths with the same dispersion exponent β . For different detection wavelengths the lifetimes are listed in Table I and vary from 10 to 70 μ s for sample s92 and from 2 to 40 μ s for sample s106 with increasing detection wavelength. The dispersion factor is $\beta=0.6$ for sample s92 and $\beta=0.54$ for s106. β does not reflect microscopic properties which depend on the size of the QD but rather a macroscopic property of the system associated with the character of the medium;¹⁴ thus the two samples consist of a difference in the structure of the SRO layer and quantum dots surface states. The stretched function is related to a

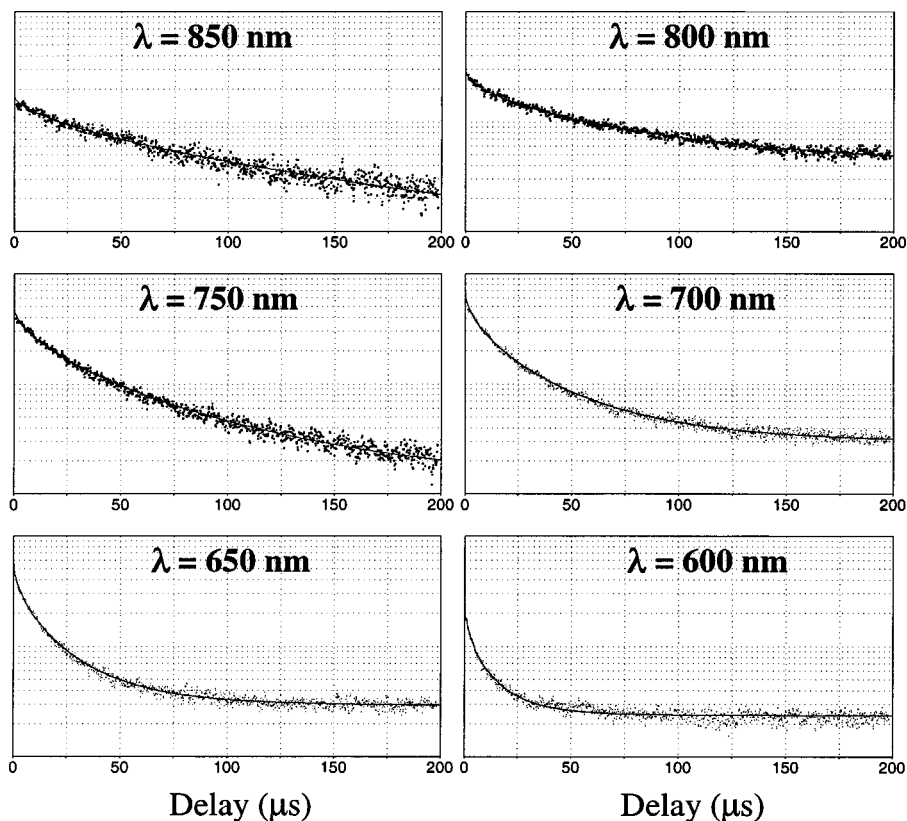


FIG. 5. Time evolution of the PL intensity for sample s92 at different detection wavelengths. The solid line shows a good fit with a stretched exponential function.

distribution of relaxation times or a time-dependent relaxation rate which reflects the interlevel relaxation processes in the QD and which will be more active in sample s106 where the separation of the dot levels is smaller. In all samples the lifetime of a high energy level is short. The plateau-like part¹⁵ in decay of low energy levels is not observed. In these samples the excited carrier in high energy level can be thermally ionized and then captured by nonradiative center.

In conclusion, time-resolved and time-integrated PL measurements have been used to study the optical properties of Si QDs. The state-filling effect and the intensity dependence of the measurements give more information about the energy structures of QDs and provide strong evidence for the origin of the observed PL. From the discussion of the degeneracy of energy dot levels we conclude that the confinement of the QDs can be described by a parabolic model. The quan-

tum confinement of Si QDs leads to an effective carrier capture and light emission in the visible range with a rather long lifetime, in the microsecond range.

TABLE I. Decay time for different detection wavelengths with $\beta=0.6$ for sample s92 and $\beta=0.54$ for sample s106.

Detection λ (nm)	600	650	700	750	800	850
s92: τ (μ s)	4	7	12	20	35	60
s106: τ (μ s)	2	4	10	18	20	55

- ¹U. Bockelmann, Phys. Rev. B **48**, 17637 (1993).
- ²S. Raymond, S. Fafard, S. Charbonneau, R. Leon, D. Leonard, P. M. Petroff, and J. L. Merz, Phys. Rev. B **52**, 17238 (1995).
- ³U. Bockelmann and T. Egeler, Phys. Rev. B **46**, 15574 (1992).
- ⁴S. Raymond *et al.*, Phys. Rev. B **54**, 11548 (1996).
- ⁵Z. H. Lu, D. J. Lockwood, and J.-M. Baribeau, Nature (London) **378**, 2580260 (1995).
- ⁶L. A. Nesbit, Appl. Phys. Lett. **46**, 38 (1985).
- ⁷E. C. Cho, Y. H. Cho, T. Trupke, R. Corkish, G. Conibeer, and M. A. Green, Paper Presented at 19th European Photovoltaic Solar Energy Conference, Paris, June 2004, and references therein.
- ⁸A. Hriciw, A. Meldrum, K. S. Buchanan, and C. W. White, Nucl. Instrum. Methods Phys. Res. B **222**, 469 (2004).
- ⁹S. Grosse *et al.*, Phys. Rev. B **55**, 4473 (1997).
- ¹⁰M. Braun, S. Link, C. Burda, and M. El-Sayed, Phys. Rev. B **66**, 205312 (2002).
- ¹¹M. Grundmann and D. Bimberg, Phys. Rev. B **55**, 9740 (1997).
- ¹²J. Tulkki and A. Heinämäki, Phys. Rev. B **52**, 8239 (1995).
- ¹³J. Kakalios, R. A. Street, and W. B. Jackson, Phys. Rev. Lett. **59**, 1037 (1987).
- ¹⁴M. Dovrat, Y. Goshen, J. Jedrzejewski, I. Balberg, and A. Saar, Phys. Rev. B **69**, 155311 (2004).
- ¹⁵W. Yang, R. R. Lowe-Webb, H. Lee, and P. C. Sercel, Phys. Rev. B **56**, 13314 (1997).